Correlation Between Cloud Adjustments and Cloud Feedbacks Responsible for Larger Range of Climate Sensitivities in CMIP6

Nicholas Lutsko[1], Matt Luongo[2], Casey James Wall[3], and Timothy A Myers[4]

[1]Scripps Institution of Oceanography.
[2]University of California, San Diego
[3]Scripps Institution of Oceanography
[4]University of Colorado Boulder

November 24, 2022

Abstract

While the higher mean Equilibrium Climate Sensitivity (ECS) in CMIP6 has been attributed to more positive cloud feedbacks, it is unclear what causes the greater range of ECS values across CMIP6 models compared to CMIP5. Here we investigate the relationship between radiative forcing and cloud feedbacks across the two model generations to explain the very high ECS values in some CMIP6 models. The relationship is sensitive to the definition of the forcing, particularly in CMIP6, but fixed-SST simulations suggest the shortwave cloud feedback ($\lambda_{SW, cl}$) is anti-correlated with the forcing in CMIP5 and weakly positively correlated with the forcing in CMIP6. These relationships reflect the cloud adjustment to the forcing, which is anti-correlated with $\lambda_{SW, cl}$ in CMIP5 and positively correlated in CMIP6. Although we are unable to identify a systematic change across the model generations, we do show that modifications to the land components of climate models are not responsible for the change in the relationship between cloud adjustments and cloud feedbacks, and that cloud adjustments are generally driven by low and, especially mid-level clouds. Moreover, models derived from the MOHC and NCAR modeling centers seem to be responsible for much of the trend between CMIP5 and CMIP6. Our analysis is severely limited by the available simulations, highlighting the need for targeted simulations to probe the sources of intermodel differences in cloud adjustments.

Correlation Between Cloud Adjustments and Cloud Feedbacks Responsible for Larger Range of Climate Sensitivities in CMIP6

Nicholas J. Lutsko[1], **Matthew T. Luongo**[1], **Casey J. Wall**[1], **Timothy A. Myers**[2,3]

[1]Scripps Institution of Oceanography, University of California at San Diego, La Jolla, California, USA.
[2]Cooperative Institute for Research in Environmental Sciences (CIRES), University of Colorado, Boulder, Colorado, USA
[3]Physical Science Laboratory, National Oceanic and Atmospheric Administration, Boulder, Colorado, USA

Key Points:

- The relationship between feedback and forcing is sensitive to the definition of the forcing, especially in CMIP6
- Cloud adjustments are anti-correlated with cloud feedbacks in CMIP5 and positively correlated in CMIP6
- It is unclear what caused this change, though models derived from a small number of modeling centers drive the trend

Corresponding author: Nicholas Lutsko, `nlutsko@ucsd.edu`

Abstract

While the higher mean Equilibrium Climate Sensitivity (ECS) in CMIP6 has been attributed to more positive cloud feedbacks, it is unclear what causes the greater range of ECS values across CMIP6 models compared to CMIP5. Here we investigate the relationship between radiative forcing and cloud feedbacks across the two model generations to explain the very high ECS values in some CMIP6 models. The relationship is sensitive to the definition of the forcing, particularly in CMIP6, but fixed-SST simulations suggest the shortwave cloud feedback ($\lambda_{SW,cl}$) is anti-correlated with the forcing in CMIP5 and weakly positively correlated with the forcing in CMIP6. These relationships reflect the cloud adjustment to the forcing, which is anti-correlated with $\lambda_{SW,cl}$ in CMIP5 and positively correlated in CMIP6. Although we are unable to identify a systematic change across the model generations, we do show that modifications to the land components of climate models are not responsible for the change in the relationship between cloud adjustments and cloud feedbacks, and that cloud adjustments are generally driven by low and, especially mid-level clouds. Moreover, models derived from the MOHC and NCAR modeling centers seem to be responsible for much of the trend between CMIP5 and CMIP6. Our analysis is severely limited by the available simulations, highlighting the need for targeted simulations to probe the sources of intermodel differences in cloud adjustments.

1 Introduction

The models participating in the Sixth Climate Model Intercomparison Project (CMIP6) have a much wider range of Equilibrium Climate Sensitivities (ECSs) than the models participating in the Fifth Climate Model Intercomparison Project (CMIP5): in CMIP6 the lowest ECS is 1.83K (INM-CM4-8) and the highest ECS is 5.64K (CanESM5), while in CMIP5 the corresponding values are 2.08K (INM-CM-4) and 4.65K (MIROC-ESM) [*Zelinka et al.*, 2020]. The high end of the CMIP6 models' ECS in particular has been the subject of much concern, as the fact that several CMIP6 models have ECS values ≥5K raises the possibility of a very high real-world ECS. While the move away from raw model weighting and towards combining multiple lines of evidence to assess ECS have led both the recent *Sherwood et al.* [2020] assessment and the IPCC's AR6 report [*Forster et al.*, 2021] to place the upper bound of ECS below 5K, it is still important to understand what causes these high sensitivities so that the realism of the models can be evaluated.

The high sensitivities also raise the possibility that models contain undiagnosed physical processes or feedbacks not included in the evaluation of *Sherwood et al.* [2020].

ECS is determined by the radiative forcing due to a doubling of CO_2, F, divided by the climate feedback parameter, or radiative restoring co-efficient, λ:

$$ECS = \frac{F}{\lambda}. \tag{1}$$

F is typically taken to include both the instantaneous radiative forcing (IRF) from increased CO_2 concentrations and the “rapid adjustments" to the forcing which appear in the first few days or weeks after CO_2 increase [*Hansen et al.*, 2005; *Gregory and Webb*, 2008; *Sherwood et al.*, 2015]. These rapid adjustments come from increases in land temperatures, decreases in stratospheric temperatures and changes in atmospheric properties that are directly forced by CO_2 and not mediated by surface temperature changes. The total feedback λ includes both clear-sky and cloud feedbacks, with the latter typically taken to be the largest source of uncertainty in ECS [e.g., *Soden et al.*, 2008; *Vial et al.*, 2013; *Forster et al.*, 2013; *Zelinka et al.*, 2020; *Sherwood et al.*, 2020].

In addition to a larger range of ECS values, the CMIP6 models also have a higher ensemble-mean ECS than the CMIP5 models. The latter was attributed by *Zelinka et al.* [2020] to a more positive ensemble-mean cloud feedback, specifically an increase in the shortwave low cloud feedback. This is driven by a more positive extratropical low cloud amount feedback and more positive SW low cloud scattering feedback in all regions [see also *Lutsko et al.*, 2021]. However, while cloud feedbacks can explain the higher mean ECS, the range of total feedbacks is similar in both sets of models, as is the range of net (longwave plus shortwave) cloud feedbacks (see Figure 1c of *Zelinka et al.* [2020]); longwave cloud feedbacks compensate to some extent for shortwave cloud feedbacks. Thus feedbacks alone cannot explain the very high ECS CMIP6 models. Instead, as Zelinka et al. note, the highest ECS models in CMIP6 combine moderate radiative forcings with weak (negative) climate feedback parameters in a way that wasn't seen in CMIP5: the most sensitive models in CMIP5 have both weak climate feedback parameters and weak forcings, which limits the maximum ECS values.

In this study, we investigate the relationships between forcings and cloud feedbacks in the two generations of models, seeking to explain why the combination of moderate forcing and small climate feedback parameter is present in some CMIP6 models but in none of the CMIP5 models. We draw on a number of previous studies that have estimated radiative forcings and feedbacks in CMIP5 and CMIP6 models (see next section) and compare different ways of estimating the radiative forcing, which turns out to be essential for clarifying the relationships between forcings and feedbacks across model generations. Our analysis is severely limited by the small number of fixed Sea Surface Temperature (SST) simulations in both ensembles, particularly CMIP5. Fixed-SST simulations are required to accurately estimate radiative forcing and to investigate what causes differences in radiative forcing between models. Nevertheless, using the available data we do find suggestive evidence that, rather than systematic differences between model generations, the changes are primarily driven by models derived from two modeling centers, which combine strong, positive cloud feedbacks and large, positive cloud adjustments to forcing.

2 Data Sources

The following data sources are used in the analysis:

- Regression-based forcing estimates, using years 1-140 of abrupt-4XCO2 simulations, for 24 CMIP5 models and 31 CMIP6 models from *Zelinka et al.* [2020].
- Shortwave cloud feedbacks ($\lambda_{SW,cl}$) for 24 CMIP5 models and 31 CMIP6 models from *Zelinka et al.* [2020].
- Regression-based forcing estimates, using years 1-20 of abrupt-4XCO2 simulations, for 24 CMIP5 models and 29 CMIP6 models from *Dong et al.* [2020].
- Fixed-SST forcing estimates for 13 CMIP5 models from *Kamae and Watanabe* [2012].
- Fixed-SST forcing estimates for 17 CMIP6 models from *Smith et al.* [2020].
- Estimates of the Cloud Radiative Effect (CRE) response to CO_2 forcing for 13 CMIP5 models from *Kamae and Watanabe* [2012]. Note that the CRE response is not equivalent to the cloud adjustment to the forcing as it does not account for cloud masking [*Soden et al.*, 2004], but it is well correlated with estimates of the true cloud adjustment (see next bullet).
- Estimates of the cloud adjustment to the forcing for six CMIP5 models (CanESM2, CCSM4, HadGEM2-A, IPSL-CM5A-LR, MIROC5 and MRI-CGCM3) are calculated following the procedure in *Zelinka et al.* [2013]. These are the models which

ran fixed-SST simulations with the ISCCP simulator[1] and thus provided the necessary data to estimate the true cloud adjustment.

- Estimates of the cloud adjustments to the forcing for 16 CMIP6 models from *Smith et al.* [2020], including 10 CMIP6 models which ran fixed-SST simulations with the ISCCP simulator. Note that we have calculated the cloud adjustment for the MIROC6 model using the *Zelinka et al.* [2013] method, which was not included in the analysis of *Smith et al.* [2020].
- Cloud adjustments in aquaplanet simulations with seven CMIP6 models, calculated following the procedure in *Zelinka et al.* [2013].
- Meteorological cloud radiative kernels from *Myers et al.* [2021] based on the Cloud Controlling Factor (CCF) analysis developed by *Scott et al.* [2020] for five CMIP5 models and seven CMIP6 models. Note that we have calculated a new CCF kernel for the CESM2 model as part of this analysis. The required meteorological data for the CCF analysis were also downloaded for each model (see Supplementary Text for more information).

See Tables 1 and 2 for complete lists of models and data used in this study. All values are linearly scaled for a doubling of CO_2, e.g., if $4XCO_2$ values are reported, we have divided them by 2.

3 Different Forcing Definitions

We begin by investigating the relationships between different forcing definitions. The simplest way of estimating radiative forcing is through so-called “Gregory" regressions [*Gregory et al.*, 2004], in which the anomalous surface temperature (T) from abrupt-4XCO2 simulations is regressed onto the anomalous net top-of-atmosphere (TOA) radiative flux (R). The forcing is defined as the y-intercept of the regression. *Zelinka et al.* [2020] diagnosed the forcings in CMIP5 and CMIP6 by regressing R onto T for years 1-140 of the abrupt-4XCO2 simulations in the two sets of simulations. These forcing estimates (F_{1-140}) are problematic, however, as the radiative feedback λ (the slope of R over T) changes over time due to the so-called “pattern effect" in which evolving patterns of

[1] The International Satellite Cloud Climatology Project (ISCCP) simulator translates modeled cloud fields into a distribution of cloud fractions as a joint function of seven cloud-top pressure ranges and seven cloud optical depth ranges, in an analogous manner to the observational ISCCP cloud product [*Klein and Jakob*, 1999; *Webb et al.*, 2001]

Table 1. CMIP5 models used in this study. Where available, regression-based forcing estimates, using years 1-140 of abrupt-4XCO2 simulations (F_{1-140}), are taken from *Zelinka et al.* [2020], regression-based forcing estimates, using years 1-20 of abrupt-4XCO2 simulations (F_{1-20}, are taken from *Dong et al.* [2020], fixed-SST forcing estimates (F_{fix}) are taken from *Kamae and Watanabe* [2012], short-wave cloud feedbacks $\lambda_{SW,cl}$ are taken from *Zelinka et al.* [2020], estimates of the Cloud Radiative Effect (CRE) response to CO_2 forcing are taken from *Kamae and Watanabe* [2012] and estimates of the cloud adjustment to the forcing are calculated following the procedure in *Zelinka et al.* [2013].

Model	F_{1-140} [Wm^{-2}]	F_{1-20} [Wm^{-2}]	F_{fix} [Wm^{-2}]	$\lambda_{SW,cl}$ [Wm^{-2}/K]	ΔCRE [Wm^{-2}]	Cloud adjustment [Wm^{-2}]
ACCESS1.0	2.94	3.56	–	0.07	–	–
ACCESS1.3	2.88	3.42	–	0.48	–	–
BCC-CSM1.1	3.24	3.78	–	-0.15	–	–
BCC-CSM1.1-M	3.43	3.85	–	-0.02	–	–
CanESM2	3.81	4.18	3.67	-0.29	-0.02	0.63
CCSM4	3.48	4.08	4.42	-0.09	0.19	0.96
CNRM-CM5	3.69	3.58	3.93	-0.21	-0.01	–
CSIRO-Mk3.6.0	2.60	3.55	3.10	0.55	-0.73	–
GFDL-CM3	3.01	3.70	–	0.6	–	–
GFDL-ESM2G	2.99	3.50	–	-0.4	–	–
GFDL-ESM2M	3.35	3.58	–	-0.49	–	–
GISS-E2-H	3.82	4.11	–	-0.72	–	–
GISS-E2-R	3.73	4.64	–	-0.8	–	–
HadGEM2-ES	2.91	3.33	3.50	0.29	-0.06	0.37
INM-CM4	2.97	3.06	3.12	-0.02	-0.57	–
IPSL-CM5A-LR	3.10	3.36	3.25	0.61	-0.28	-0.05
IPSL-CM5A-MR	3.31	3.50	–	0.62	–	–
IPSL-CM5B-LR	2.65	3.03	–	0.35	–	–
MIROC5	4.16	4.38	3.97	-0.38	-0.21	0.61
MPI-ESM-LR	4.10	4.58	4.31	-0.16	0.10	–
MPI-ESM-MR	4.11	4.68	4.30	-0.07	0.12	–
MPI-ESM-P	4.27	4.91	4.30	-0.21	0.11	–
MRI-CGCM3	3.20	3.60	3.60	0.25	-0.42	0.06
NorESM1-M	3.16	3.77	3.48	-0.02	0.04	–

Table 2. CMIP6 models used in this study. Where available, regression-based forcing estimates, using years 1-140 of abrupt-4XCO2 simulations (F_{1-140}), are taken from *Zelinka et al.* [2020], regression-based forcing estimates, using years 1-20 of abrupt-4XCO2 simulations (F_{1-20}), are taken from *Dong et al.* [2020], fixed-SST forcing estimates (F_{fix}) are taken from *Smith et al.* [2020], short-wave cloud feedbacks $\lambda_{SW,cl}$ are taken from *Zelinka et al.* [2020], estimates of the cloud adjustment to the forcing are taken from *Smith et al.* [2020] and estimates of the cloud adjustment in aquaplanet simulations are calculated following the procedure in *Zelinka et al.* [2013]

Model	F_{1-140} [Wm^{-2}]	F_{1-20} [Wm^{-2}]	F_{fix} [Wm^{-2}]	$\lambda_{SW,cl}$ [Wm^{-2}/K]	Cloud adjustment [Wm^{-2}]	Aquaplanet cloud adjustment [Wm^{-2}]
ACCESS-CM2	3.43	4.12	3.97	0.96	0.70	–
ACCESS-ESM1-5	2.83	3.50	–	0.43	–	–
BCC-CSM2-MR	3.11	3.59	–	0.16	–	–
BCC-ESM1	3.01	3.47	–	0.02	–	–
CAMS-CSM1.0	4.17	4.33	–	-0.72	–	–
CESM2-WACCM	3.30	4.05	—	1.05	–	–
CESM2	3.27	4.18	4.45	0.79	1.07	1.62
CNRM-CM6.1	3.64	3.95	4.00	-0.02	0.22	0.20
CNRM-ESM2.1	2.97	2.79	3.96	0.03	0.12	–
CanESM5	3.68	3.75	3.80	-0.02	0.47	–
E3SM-1.0	3.33	3.68	–	0.75	–	–
EC-Earth3-Veg	3.22	4.00	–	0.02	–	–
EC-Earth3	3.37	4.00	4.05	0.05	–	–
GFDL-CM4	3.19	4.23	4.22	0.03	0.56	0.52
GFDL-ESM4	3.77	3.69	3.87	-0.15	0.62	–
GISS-E2.1-G	3.95	4.00	3.67	-0.63	0.12	–
GISS-E2.1-H	3.53	3.72	–	-0.53	–	–
HadGEM3-GC31-LL	3.49	3.87	4.05	0.98	0.74	0.58
INM-CM4.8	2.70	3.13	–	-0.19	–	–
INM-CM5.0	2.92	3.14	—	-0.11	–	–
IPSL-CM6A-LR	3.58	3.90	4.00	0.14	0.47	0.16
MIROC-ES2L	4.11	3.98	–	-0.35	–	–
MIROC6	2.65	3.65	3.66	-0.13	0.35	0.47
MPI-ESM1.2-LR	4.22	–	4.17	-0.68	0.70	–
MPI-ESM1.2-HR	3.65	4.18	–	-0.41	–	–
MRI-ESM2.0	3.43	3.99	3.83	0.12	0.29	0.72
NESM3	3.73	4.91	–	-0.15	–	–
NorESM2-LM	3.43	4.61	4.07	0.21	0.72	–
NorESM2-MM	3.73	–	4.19	0.30	0.78	–
SAM0-UNICON	3.89	4.18	–	0.89	–	–
UKESM1.0-LL	3.61	3.82	3.97	0.93	0.80	–

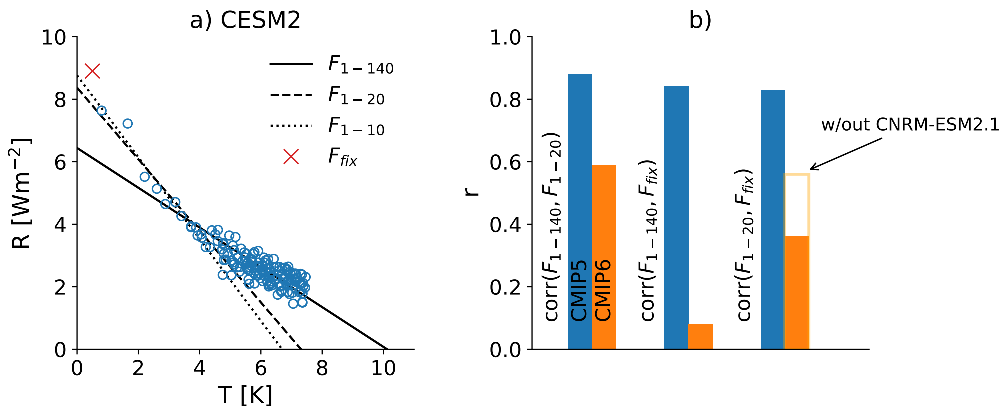

Figure 1. a) "Gregory" plot of R against T for a representative CMIP6 model (CESM2). The blue markers show annual-mean values, the solid line shows a regression of R against T using all 140 years of data, the dashed line shows a regression using only years 1-20 and the dotted line shows a regression using years 1-20. The regression-based forcings are taken to be the y-intercepts of these lines. The red cross shows the fixed-SST forcing F_{fix}. b) Pearson correlation coefficients (r) between the different forcing estimates for the CMIP5 data (blue) and the CMIP6 (orange). The empty orange bar in the third column shows r when CNRM-ESM2.1 (whose abrupt4XCO2 simulation was set up incorrectly, leading to an anomalously small F_{1-20}) is excluded from the correlation.

warming cause λ to change over time [*Winton et al.*, 2010; *Armour et al.*, 2013; *Geoffroy et al.*, 2013; *Andrews et al.*, 2015; *Xie*, 2020]. Plots of R against T typically feature inflection points about 20 years after the increase in CO_2 and so, since λ decreases over time, regressing over all 140 years will typically lead to an underestimate of F (see Figure 1a). For the same reason, F_{1-140} will tend to be correlated across models with λ: a model with a smaller (less negative) λ will have a smaller F_{1-140}. The correlation between λ and F_{1-140} further implies a correlation between F_{1-140} and $\lambda_{SW,CL}$, since $\lambda_{SW,CL}$ is the main source of uncertainty in λ. This partly explains the statistically significant correlations between F and $\lambda_{SW,CL}$ found in previous studies [see below and e.g., *Caldwell et al.*, 2016].

To obtain forcing estimates that do not depend so directly on λ, we consider two other ways of estimating F. First, F can be diagnosed by regressing T onto R over the first 20 years of the abrupt 4XCO2 simulations (F_{1-20}), as used e.g., by *Dong et al.* [2020]. These estimates are more independent of the feedback but, as noted by *Forster et al.* [2016], regression-based estimates of F are sensitive to the number of years included in the regressions: F_{1-10} will differ slightly from F_{1-20} (see Figure 1a). Second, we take estimates of F from simulations in which atmospheric CO_2 concentrations are quadrupled but SSTs are kept fixed (F_{fix}). Taking the difference between these and control simulations gives forcing estimates that include both the IRF and the rapid adjustments. F_{fix} does not depend explicitly on λ and is not sensitive to the number of years included in the analysis provided that the forcing is estimated over a long enough time period for internal variability to be small.

In CMIP5 these three sets of forcing estimates are well correlated (blue bars in Figure 1b), though F_{1-140} is almost always smaller than F_{1-20} and F_{fix} (Supplemental Figure S1). By contrast, in CMIP6 the correlation between F_{1-140} and F_{1-20} is much lower and the correlation between F_{1-140} and F_{fix} is negligible (orange bars in Figure 1b). F_{1-20} and F_{fix} are weakly correlated in CMIP6 (r = 0.36), though note that the 4XCO2 simulations with CNRM-ESM2.1 were not set up correctly [*Smith et al.*, 2020], leading to an anomalously small value of F_{1-20} (see panel e of Supplemental Figure S1). Without this outlier model, the correlation between F_{1-20} and F_{fix} is substantially higher (r = 0.56). Hereafter, we take F_{1-20} and F_{fix} to be more representative of models' true radiative forcings than the F_{1-140} estimates used by *Zelinka et al.* [2020].

4 Relationships Between Forcings and Cloud Feedbacks

We now examine the relationship between F and $\lambda_{SW,CL}$ in the two sets of models. Figure 2a-c shows that whatever forcing definition is used, F and $\lambda_{SW,CL}$ are anti-correlated in the CMIP5 models [see also *Caldwell et al.*, 2016]. That is, even F_{1-20} and F_{fix}, which are not directly related to the long-term value of λ, have an inverse relationship with $\lambda_{SW,CL}$ in the CMIP5 models.

By contrast, there is no relationship between F_{1-20} and $\lambda_{SW,CL}$ in the CMIP6 models (r = 0.05, Figure 2e), while F_{fix} and $\lambda_{SW,CL}$ are weakly positively correlated (r = 0.37, Figure 2f). F_{1-140} and $\lambda_{SW,CL}$ are anti-correlated in CMIP6, as expected from the discussion in the previous section (Figure 2d), though the relationship is much weaker than in CMIP5 (r = -0.25 versus r = -0.61). Given the discussion above and in *Forster* [2016], we take the fixed SST estimates to be the most reliable forcing estimates, such that the forcing and the SW cloud feedback are anti-correlated in CMIP5 and weakly positively correlated in CMIP6.

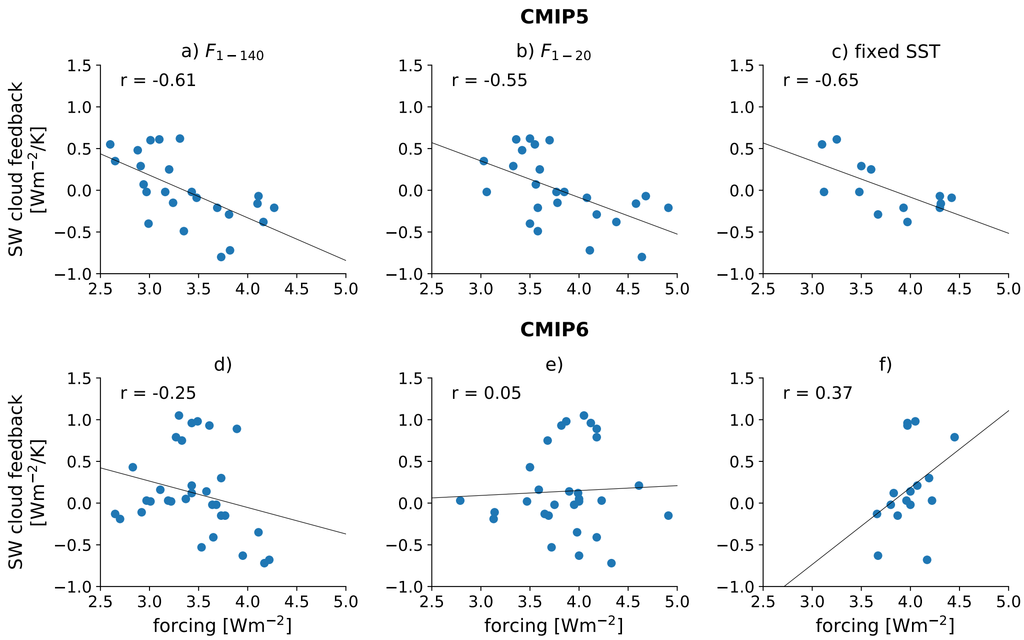

Figure 2. Relationships between the SW cloud feedback $\lambda_{SW,cl}$ and different forcing definitions in CMIP5 and CMIP6. a) $\lambda_{SW,cl}$ versus F_{1-140} in CMIP5, b) $\lambda_{SW,cl}$ versus F_{1-20} in CMIP5, c) $\lambda_{SW,cl}$ versus F_{fix} in CMIP5, d) $\lambda_{SW,cl}$ versus F_{1-140} in CMIP6, e) $\lambda_{SW,cl}$ versus F_{1-20} in CMIP6, f) $\lambda_{SW,cl}$ versus F_{fix} in CMIP6. In all panels the Pearson correlation coefficient r is shown in the upper left and the lines show linear least-squares regressions.

5 Cloud Adjustments and Cloud Feedbacks

The most likely candidate to explain the relationships between forcings and cloud feedbacks is the cloud adjustment to the forcing. Unfortunately, only six modeling centers ran fixed SST simulations with ISCCP simulators in CMIP5, which are needed to estimate the cloud adjustments using the *Zelinka et al.* [2013] methodology. For this reason, we have also used the change in Cloud Radiative Effect (ΔCRE), as diagnosed for 13 CMIP5 models by *Kamae and Watanabe* [2012], to investigate the relationships between cloud adjustments, total forcings and cloud feedbacks. 10 CMIP6 models ran fixed SST simulations with the ISCCP simulator, and *Smith et al.* [2020] estimated the forcing for six additional models using other methods (the approximate partial radiative perturbation method and the offline monthly-mean partial radiative perturbation method).

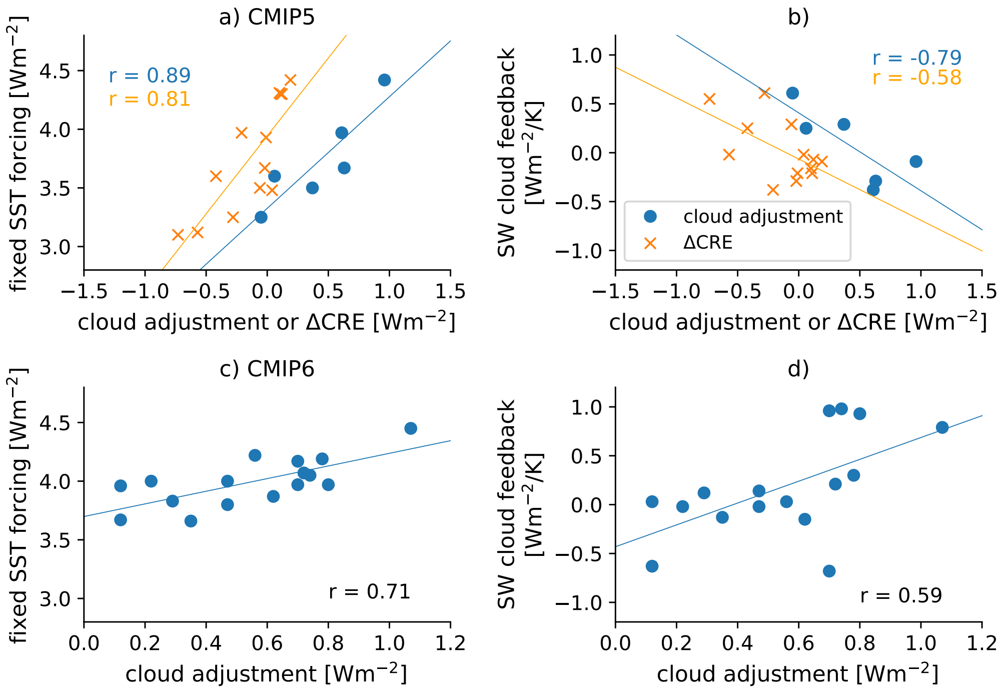

Figure 3. Relationships between cloud adjustments, the fixed-SST forcings and the SW cloud feedbacks. a) Fixed SST forcing F_{fix} versus the cloud adjustment in CMIP5 (blue circles), and versus the change in CRE in fixed-SST CMIP5 simulations (orange crosses). b) SW cloud feedback $\lambda_{SW,cl}$ versus the cloud adjustment in CMIP5 (blue circles), and versus the change in CRE in fixed-SST CMIP5 simulations (orange crosses). c) Fixed SST forcing F_{fix} versus the cloud adjustment in CMIP6. d) SW cloud feedback $\lambda_{SW,cl}$ versus the cloud adjustment in CMIP6. The Pearson correlation coefficients are indicated on each panel and the lines show linear least-squares regressions.

The cloud adjustment is positively correlated with the forcing and anti-correlated with the SW cloud feedback in CMIP5, consistent with the results of the previous section (Figure 3a-b). IPSL-CM5A-LR, which has the largest SW cloud feedback, has a small, negative cloud adjustment, while CCSM4 has the largest cloud adjustment and a negative SW cloud feedback (see Table 1). This anti-correlation was also noted for CMIP5 by *Chung and Soden* [2015], though they examined the CRE responses for both the adjustments and the feedbacks in CMIP5, not the “true" cloud adjustments and cloud feedbacks. In CMIP6 the cloud adjustment is positively correlated with both the fixed-SST forcing estimates (Figure 3c) and the SW cloud feedbacks (Figure 3d). Interestingly, in CMIP6

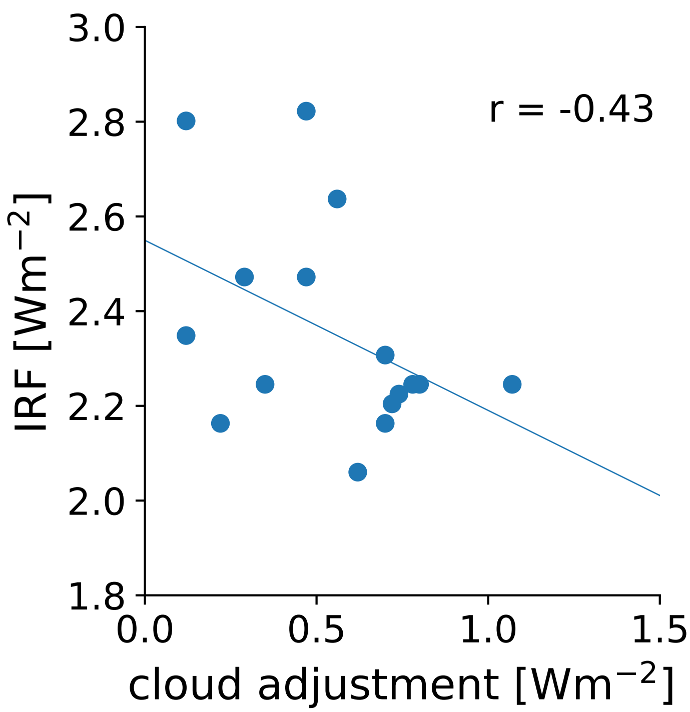

Figure 4. Cloud adjustment versus IRF in the 16 CMIP6 models analyzed by *Smith et al.* [2020]. The Pearson correlation coefficient is given in the top right and the line shows the linear least-square regression.

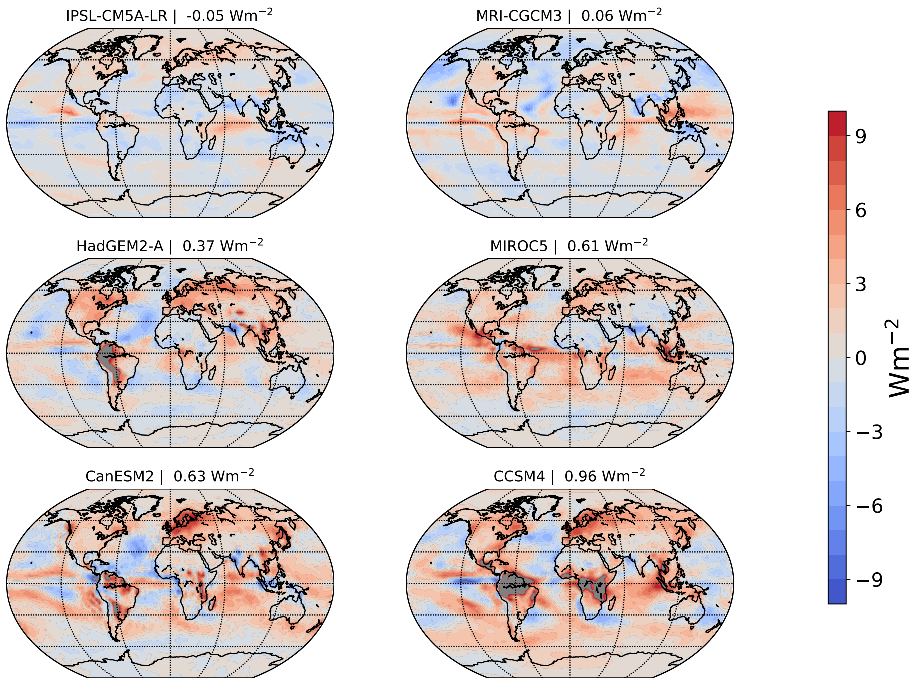

Figure 5. Spatial maps of the net cloud adjustments in the six CMIP5 models which ran fixed-SST simulations with the ISCCP simulator. The global-mean net cloud adjustment is given above each panel, and the models are ordered by the size of their adjustment. Values outside the colorbar range are shaded in gray.

the cloud adjustment is anti-correlated with the IRF (r = -0.43, Figure 4). We have not investigated this relationship further, and note that *Andrews et al.* [2019] mentioned the possibility of such an anti-correlation in their investigation of the causes of higher sensitivity in the HadGEM3-GC3.1-LL climate model. Anti-correlation between IRF and cloud adjustments may explain why the relationships between the SW cloud feedback and the total forcing metrics are weak in CMIP6, even though there is a more robust relationship between $\lambda_{SW,cl}$ and the cloud adjustments: since the total forcing is largely set by the sum of the IRF and the cloud adjustment, anti-correlation between these may reduce the correlation between the total forcing and the SW cloud feedback.

6 What Changed Between CMIP5 and CMIP6?

The relatively small number of fixed-SST simulations, especially in the CMIP5 archive, makes it difficult to uncover systematic differences between the two generations of models. Moreover, cloud adjustments remain poorly understood compared to cloud feedbacks, though it is known that they are driven by land-sea circulations and changes

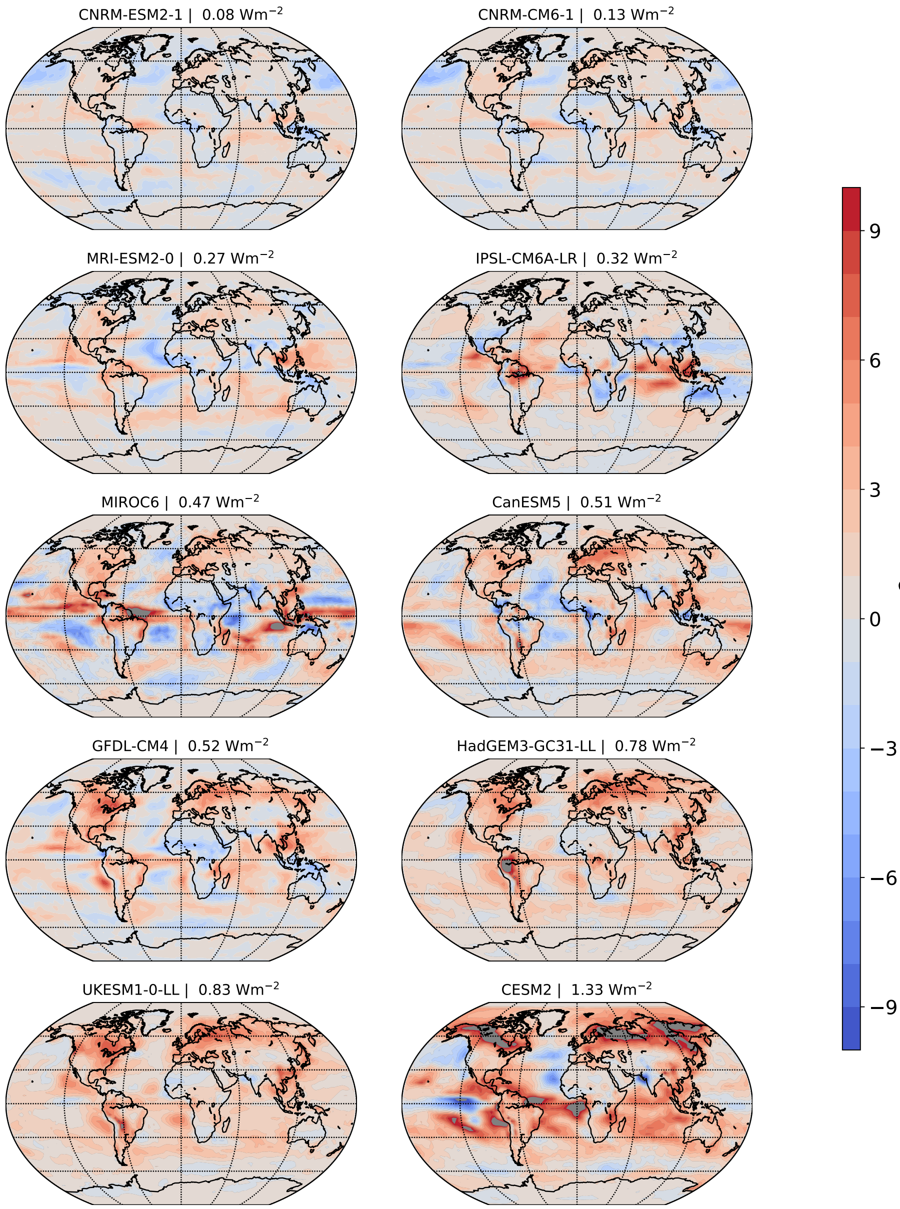

Figure 6. Spatial maps of the net cloud adjustments in the ten CMIP6 models which ran fixed-SST simulations with the ISCCP simulator. The global-mean net cloud adjustment is given above each panel, and the models are ordered by the size of their adjustment. Values outside the colorbar range are shaded in gray. Note that in some cases the global-mean cloud adjustments differ from the values in Table 2, which are the average of the three methods used by *Smith et al.* [2020] to estimate cloud adjustments, whereas the values in this figure only come from the *Zelinka et al.* [2013] method.

in atmospheric stability, among other things. There is also a diverse range of cloud adjustment patterns across the models, and comparing the cloud adjustments in the six modeling centers which provided fixed-SST simulations in both CMIP5 and CMIP6 (CCCMA, IPSL NCAR, MIROC, MOHC, MRI) shows that the patterns of cloud adjustments are more similar for models from the same modeling center than for models from the same generation (compare relevant panels in Figures 5 and 6).

Changes in cloud adjustments are also not obviously connected to changes in cloud feedbacks: $\lambda_{SW,cl}$ increased substantially in the two NCAR models (by +0.88Wm^{-2}/K) and in the two MOHC models (by +0.69Wm^{-2}/K), increased to a lesser extent in the MIROC and CCCma models (by +0.25Wm^{-2}/K and +0.07Wm^{-2}/K, respectively) and decreased in the MRI and IPSL models (by -0.13Wm^{-2}/K and -0.47Wm^{-2}/K, respectively), while the largest increase in cloud adjustment is seen between the two IPSL models (+0.52Wm^{-2}), then between the two MOHC models (+0.37 Wm^{-2}), between the MRI models (+0.23 Wm^{-2}) and the NCAR models (+0.11 Wm^{-2}). The net cloud adjustment decreased by -0.16Wm^{-2} between the CCCMa models and by -0.25Wm^{-2} between the MIROC models (Figures 5 and 6). Hence changes in cloud adjustments cannot be predicted by changes in cloud feedbacks.

Nevertheless, we have worked with the available data to explore potential explanations for the changes in behavior between the model generations. The first possibility we investigated is that modifications to the land components of the models are responsible for the changes between generations. We have also decomposed the net cloud adjustments into contributions from different cloud types and used a cloud controlling factor analysis to probe the causes of changes in low clouds. While neither analysis has shown conclusively what changed between the model generations, these calculations have allowed us to rule out certain possibilities and to identify key features of the changes between model generations.

6.1 Changes in land models

Cloud adjustments are partly the result of circulations which arise due to differential warming of land surfaces and the ocean [assuming SSTs are kept fixed *Andrews et al.*, 2012; *Zelinka et al.*, 2013]. Between CMIP5 and CMIP6, the land components of many

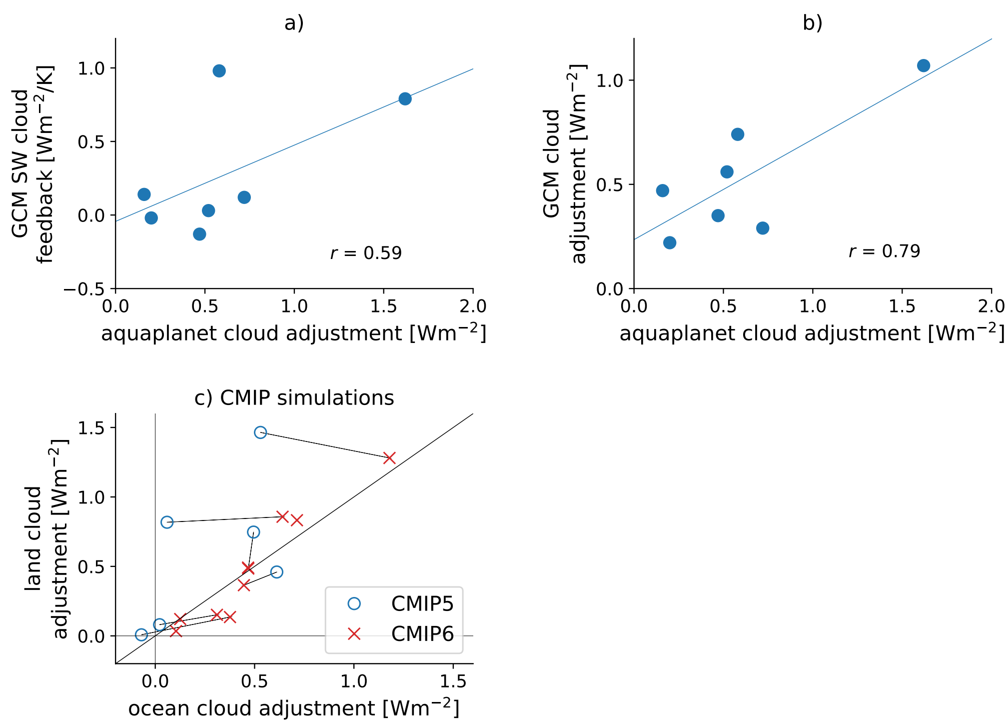

Figure 7. a) Cloud adjustments in the aquaplanet CMIP6 simulations versus the SW cloud feedback. The blue line shows a linear least-squares regression. b) Cloud adjustments in the aquaplanet CMIP6 simulations versus the true cloud adjustments calculated from the fixed SST simulations. The blue line shows a linear least-squares regression.c) Land and ocean contributions to the cloud adjustments in the comprehensive simulations. CMIP5 models are denoted by the open blue circles and CMIP6 models by the red crosses. The diagonal black line shows the 1:1 line.

models were upgraded, which could drive changes in cloud adjustments between the generations.

We have investigated this possibility in two ways. First, we calculated the cloud adjustments in aquaplanet simulations with seven CMIP6 models which outputted ISCCP data. These cloud adjustments are independent of land models, and can be compared with the results of *Ringer et al.* [2014], who found an anti-correlation between the CRE adjustments and the CRE responses in aquaplanet simulations with a subset of CMIP5 models. In CMIP6, the cloud adjustments are positively correlated with $\lambda_{SW,CL}$ in the aquaplanet simulations (r = 0.59, Figure 7a), and these adjustments are also well correlated with the cloud adjustments in the Earth-like simulations (r = 0.81, Figure 7b). *Qin et al.* [2022] found a similar change in the sign of the relationship between the CRE responses to CO_2 forcing and the CRE feedbacks in the CMIP5 and CMIP6 aquaplanet simulations (see their Table 1).

Second, we decomposed the total cloud adjustments in the comprehensive model simulations into contributions over land regions and over ocean regions (Figure 7c). There are no systematic differences in the magnitudes of the cloud adjustments over land between the generations, though comparing the cloud adjustments in the six modeling centers which provided fixed-SST simulations in both CMIP5 and CMIP6 shows that the adjustment over ocean is always larger in CMIP6 than in the corresponding CMIP5 model. The CMIP6 models cluster more closely to the 1:1 line than the CMIP5 models.

Together, these two lines of evidence strongly suggest that changes in land models are not responsible for the differences in cloud adjustments between the model generations, which are instead likely driven by changes in atmospheric physics.

6.2 Contributions of different cloud types

To better understand the nature of the cloud adjustments, we decomposed the net adjustments into the longwave and shortwave components (LW and SW, respectively; left panels of Figure 8). The SW component is substantially larger than the LW component in all of the models, with the exception of IPSL-CM5A-LR, suggesting that low and/or mid-level clouds are primarily driving the adjustments. This is confirmed in the right panels of Figure 8, in which the adjustments are decomposed into contributions from low clouds (bottom two levels of the *Zelinka et al.* [2013] cloud kernels, 900-740hPa mid-points),

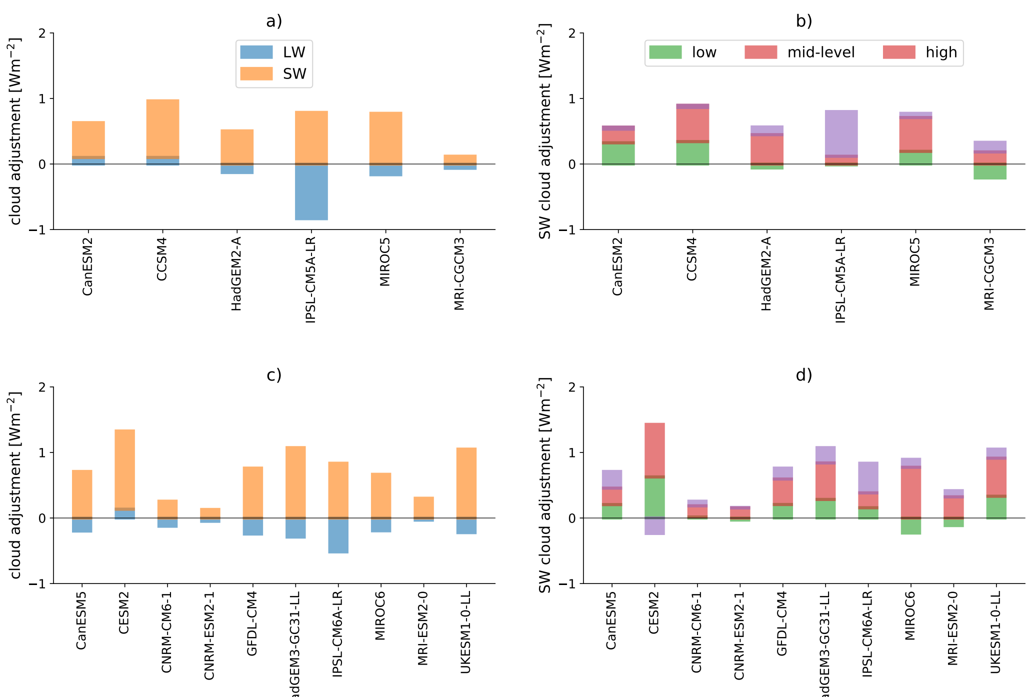

Figure 8. a) Decomposition of the total cloud adjustment into longwave (LW, blue) and shortwave (SW, orange) in the CMIP5 models. b) Decomposition of the SW cloud adjustment into contributions from low (green), mid-level (red) and high (purple) clouds in the CMIP5 models. c) Same as panel a) but for the CMIP6 models. d) Same as pandel b) but for the CMIP6 models.

mid-level clouds (levels 3 and 4 of the cloud kernels, 620-500hPa mid-points) and high clouds (375hPa mid-point and above). Mid-level clouds are responsible for most of the intermodel differences in cloud adjustments, with smaller contributions from low clouds. The high cloud contribution is generally weak, except for in the IPSL models, particularly IPSL-CM5A-LR. We have not investigated why high clouds are so important for the adjustment in these models.

While it is difficult to further determine what causes intermodel variations in mid-level cloud adjustments, we are able to provide some insight into the low cloud adjustments. This is helpful because the three CMIP6 models with the highest ECS values included here – CESM2, HadGEM3-GCM31-LL and the UKESM1-0-LL – have the three largest low cloud adjustments. Cloud Controlling Factors (CCFs) can be used to investigate how changes in governing meteorological conditions contribute to the large low cloud adjustments in these models (*Klein et al.* [2018], see Supplemental Material for more details), and the residual between the true cloud adjustments and the CCF-derived adjustments can be taken as an estimate of CO_2's direct effect on low clouds. [As part of this analysis we have calculated the low cloud adjustments following *Scott et al.* [2020], which slightly modifies the *Zelinka et al.* [2013] method to remove the effects of mid- and high-level cloud masking. These estimates of the adjustments are qualitatively similar to the Zelinka et al.-derived estimates, but provide a more accurate estimate of the CO_2 direct effect.]

Figure 9 compares the true cloud adjustments in all of the available models, the CCF-derived low cloud adjustment estimates, and our estimates of the CO_2 direct effects. Also shown are the contributions of changes in Estimated Inversion Strength (EIS) to the CCF cloud adjustment. The complete CCF breakdown is shown in Supplemental Figure S2.

In all of the models, the CCF analysis suggests the low cloud adjustment will be negative (blue bars in panels a and b of Figure 9), and that this is largely driven by EIS changes – since surface temperatures are fixed, radiative heating in the free troposphere increases EIS, which in turn increases low cloud cover. Large CO_2 direct effect contributions counter the EIS component, leading to the generally positive low cloud adjustments (red bars in panels a and b of Figure 9). The inferred low cloud reduction as a direct effect of increasing CO_2 is consistent with theory and large eddy simulations, establishing

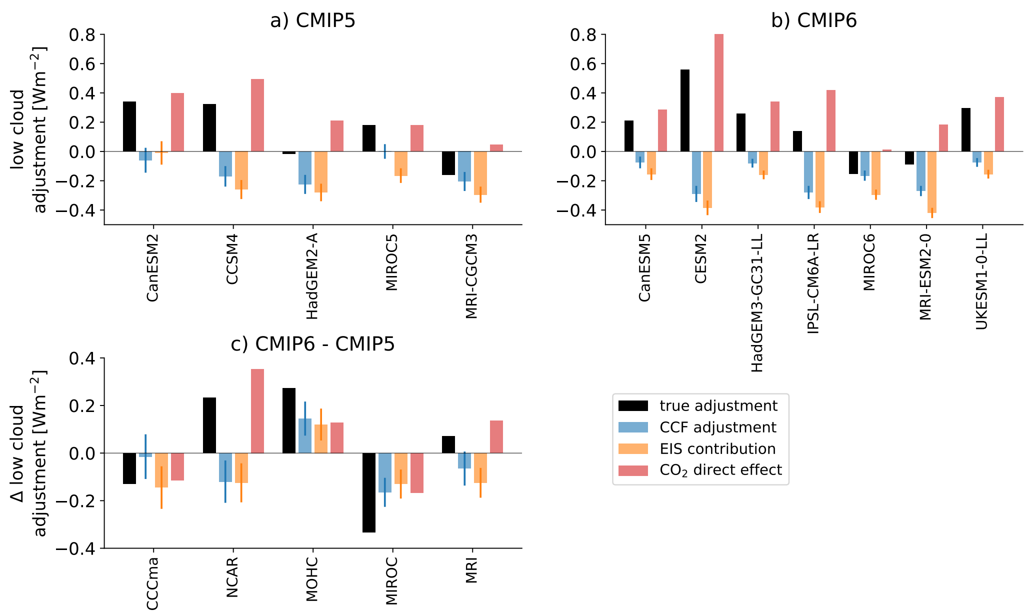

Figure 9. a) Results of cloud controlling factor anaysis for available CMIP5 data. Black bars show the "true" low cloud adjustments, calculated following *Scott et al.* [2020], blue bars show the CCF-derived cloud adjustments, orange bars show the EIS contribution to the CCF-derived cloud adjustments and red bars show the estimates CO_2 direct effect (difference between black and blue bars). b) Same as a) but for the available CMIP6 data. c) Differences between CMIP6 and CMIP5 models from the same modeling centers. The method for estimating the errorbars is described in the Appendix, and the error bars in panel c are calculated by adding the individual errors of two given models in quadrature.

confidence in our method for diagnosing its contribution to the overall low cloud adjustment [*Bretherton*, 2015; *Tan et al.*, 2017; *Sherwood et al.*, 2020]. Increasing CO_2 reduces cloud-top radiative cooling and hence the turbulent mixing within the boundary layer, resulting in reduced stratiform cloudiness.

Comparing the results for the five modeling center which provided the required data for both the CMIP5 and CMIP6 models (CCF kernels are not available for the IPSL-CM5A-LR model) shows large variations in the intergenerational differences (Figure 9c). For example, the two models with the largest increases in low cloud adjustment, CESM2 and HadGEM, achieve this in different ways. In CESM2 the sensitivity to EIS actually increases – implying a more negative cloud adjustment – but this is countered by a much stronger CO2 direct effect. In HadGEM3 the sensitivity to EIS decreases and the sensitivity to CO2's direct effect increases, both contributing approximately equally to the total increase in the cloud adjustment.

7 Summary and Discussion

In this study, we have investigated the causes of the larger range of ECS values in CMIP6 compared to CMIP5. This required clarifying the definition of the radiative forcing: estimates of the forcing obtained by performing Gregory regressions for years 1-140 of abrupt-4XCO2 simulations are influenced by models' long-term feedbacks and tend to exhibit an apparent anti-correlation between the forcing and the SW cloud feedback. Instead, using more accurate estimates of the forcing derived from fixed-SST simulations, we found that the cloud adjustment to the forcing and the SW cloud feedback are anti-correlated in CMIP5, while in CMIP6 the relationship is weakly positive. In turn, the SW cloud feedback and the forcing are negatively correlated in CMIP5 and weakly positively correlated in CMIP6 (the cloud adjustment is anti-correlated with the IRF in CMIP6, weakening the relationship between the forcing and the SW cloud feedback). The anti-correlation in CMIP5 damps the high end of ECS, as a model with a strong positive cloud feedback will have a smaller cloud adjustment and reduced forcing, whereas the CMIP6 models with strong cloud feedbacks and large cloud adjustments have high ECS values over 5K.

We have been unable to identify a single factor responsible for the change between the two model generations, though our analysis was limited by the small number of fixed

SST simulations available for probing cloud adjustments. By calculating the cloud adjustments for aquaplanet simulations with CMIP6 models, we have shown that differences in atmospheric physics, and not in the the representation of land processes, are likely responsible for the opposite behavior in the two model generations. Furthermore, the differences in cloud adjustments across models are primarily driven by low and, especially, mid-level clouds, with the exception of the IPSL models for which high clouds make a larger contribution. We have used a Cloud Controlling Factor analysis to investigate the low cloud adjustments, and found that a negative EIS and a positive contribution from the CO_2 direct effect are the largest two components of the overall low cloud adjustment. However, these two factors vary substantially across models and there are no clear trends between the model generations.

Many of the trends identified here are driven by a small number of models: CESM2, HadGEM3-GCM31-LL and UKESM1-0-LL all have large, positive SW cloud feedbacks and cloud adjustments. Most of the other CMIP6 models with ECS values above 5K were originally derived from either the NCAR or MOHC models (e.g., E3SM and CIESM), as is UKESM1-0-LL. *Knutti et al.* [2013] has shown that models derived from the same original model can retain similarities for several generations, thus it may be that all the models originally derived from those two modeling centers experienced a change in the sign of the relationship between cloud adjustments and cloud feedbacks between CMIP5 and CMIP6, which expanded the range of ECS between the model generations. An important exception, which merits further study, is the CanESM5 model, which has an ECS above 5K, a moderate cloud adjustment, a relatively large total forcing and a relatively small net feedback that is largely driven by the LW cloud feedback, not the SW cloud feedback. In general, we believe that the results presented above argue for more simulations designed to probe the mechanisms of cloud adjustments and hence improve our understanding of what caused the greater range of ECS values in the CMIP6 generation of models.

Acknowledgments

We thank Chris Smith for sharing the CMIP6 cloud adjustment data and Masahiro Watanabe and Miki Arai for sharing the MIROC6 fixed SST data. We also thank Tim Andrews for the suggestion to calculate the cloud adjustments for the aquaplanet simulations and Nadir Jeevanjee for helpful discussions. N.J.L. and C.J.W. were supported by the NOAA

Climate Program Office's Modeling, Analysis, Predictions, and Projections program through grant NA20OAR4310387.

Open Research

All CMIP data are available from the ESGF at *LLNL* [2022]. The cloud kernels used to calculate the adjustments are available at *Zelinka* [2022] and the meteorological cloud radiative kernels used in the CCF analysis are available at *Myers* [2022]. All analysis and processing scripts will be made publicly available upon acceptance of the paper.

References

Andrews, T., J. M. Gregory, M. J. Webb, and K. E. Taylor (2012), Forcing, feedbacks and climate sensitivity in cmip5 coupled atmosphere-ocean climate models, *Geophysical Research Letters*, *39*(9), l09712.

Andrews, T., J. M. Gregory, and M. J. Webb (2015), The dependence of radiative forcing and feedback on evolving patterns of surface temperature change in climate models., *Journal of Climate*, *28*(2), 1630–1648.

Andrews, T., M. B. Andrews, A. Bodas-Salcedo, G. S. Jones, T. Kuhlbrodt, J. Manners, M. B. Menary, J. Ridley, M. A. Ringer, A. A. Sellar, C. A. Senior, and Y. Tang (2019), Forcings, feedbacks, and climate sensitivity in hadgem3-gc3.1 and ukesm1, *Journal of Advances in Modeling Earth Systems*, *11*(12), 4377–4394, doi: https://doi.org/10.1029/2019MS001866.

Armour, K. C., C. M. Bitz, and G. H. Roe (2013), Time-Varying Climate Sensitivity from Regional Feedbacks, *Journal of Climate*, *26*(13), 4518–4534, doi:10.1175/JCLI-D-12-00544.1.

Bretherton, C. S. (2015), Insights into low-latitude cloud feedbacks from high-resolution models, *Philosophical Transactions of the Royal Society A: Mathematical, Physical and Engineering Sciences*, *373*(2054), 20140,415.

Caldwell, P. M., M. D. Zelinka, K. E. Taylor, and K. Marvel (2016), Quantifying the Sources of Intermodel Spread in Equilibrium Climate Sensitivity, *Journal of Climate*, *29*(2), 513–524, doi:10.1175/JCLI-D-15-0352.1, publisher: American Meteorological Society Section: Journal of Climate.

Chung, E.-S., and B. J. Soden (2015), An Assessment of Direct Radiative Forcing, Radiative Adjustments, and Radiative Feedbacks in Coupled OceanâĂŞAtmosphere Models, *Journal of Climate*, *28*(10), 4152–4170, doi:10.1175/JCLI-D-14-00436.1, publisher: American Meteorological Society Section: Journal of Climate.

Dong, Y., K. C. Armour, M. D. Zelinka, C. Proistosescu, D. S. Battisti, C. Zhou, and T. Andrews (2020), Intermodel Spread in the Pattern Effect and Its Contribution to Climate Sensitivity in CMIP5 and CMIP6 Models, *Journal of Climate*, *33*(18), 7755–7775, doi:10.1175/JCLI-D-19-1011.1, publisher: American Meteorological Society Section: Journal of Climate.

Forster, P., T. Storelvmo, K. Armour, W. Collins, J.-L. Dufresne, D. Frame, D. J. Lunt, T. Mauritsen, M. D. Palmer, M. Watanabe, M. Wild, and H. Zhang (2021), The earthâĂŹs energy budget, climate feedbacks, and climate sensitivity, in *Climate Change 2021: The Physical Science Basis. Contribution of Working Group I to the Sixth Assessment Report of the Intergovernmental Panel on Climate Change*, edited by V. Masson-Delmotte, P. Zhai, A. Pirani, S. L. Connors, C. Péan, S. Berger, N. Caud, Y. Chen, L. Goldfarb, M. I. Gomis, M. Huang, K. Leitzell, E. Lonnoy, J. B. R. Matthews, T. K. Maycock, T. Waterfield, O. Yelekci, R. Yu, and B. Zhou, Cambridge University Press, Geneva, Switzerland.

Forster, P. M. (2016), Inference of climate sensitivity from analysis of earthâĂŹs energy budget, *Annual Reviews of Earth and Planetary Sciences*, *44*(0), 85–106.

Forster, P. M., T. Andrews, P. Good, J. M. Gregory, L. S. Jackson, and M. Zelinka (2013), Evaluating adjusted forcing and model spread for historical and future scenarios in the cmip5 generation of climate models, *Journal of Geophysical Research: Atmospheres*, *118*, 1139–1150.

Forster, P. M., T. Richardson, A. C. Maycock, C. J. Smith, B. H. Samset, G. Myhre, T. Andrews, R. Pincus, and M. Schulz (2016), Recommendations for diagnosing effective radiative forcing from climate models for CMIP6, *Journal of Geophysical Research: Atmospheres*, *121*(20), 12,460–12,475, doi:10.1002/2016JD025320, _eprint: https://onlinelibrary.wiley.com/doi/pdf/10.1002/2016JD025320.

Geoffroy, O., D. Saint-Martin, G. Bellon, A. Voldoire, D. J. L. Olivie, and S. Tyteca (2013), Transient climate response in a two-layer energy-balance model. part ii: Representation of the efficacy of deep-ocean heat uptake and validation for cmip5 aogcms, *Journal of Climate*, *26*(6), 1859–1876.

Gregory, J., and M. Webb (2008), Tropospheric adjustment induces a cloud component in co_2 forcing, *Journal of Climate*, *21*(1), 58–71.

Gregory, J. M., W. J. Ingram, M. A. Palmer, G. S. Jones, P. A. Stott, R. B. Thorpe, J. A. Lowe, T. C. Johns, and K. D. Williams (2004), A new method for diagnosing radiative forcing and climate sensitivity, *Geophysical Research Letters*, *31*, L03,205.

Hansen, J., M. Sato, R. Ruedy, L. Nazarenko, A. Lacis, G. A. Schmidt, G. Russell, I. Aleinov, M. Bauer, S. Bauer, N. Bell, B. Cairns, V. Canuto, M. Chandler, Y. Cheng, A. Del Genio, G. Faluvegi, E. Fleming, A. Friend, T. Hall, C. Jackman, M. Kelley, N. Y. Kiang, D. Koch, J. Lean, J. Lerner, K. Lo, S. Menon, R. L. Miller, P. Minnis, T. Novakov, V. Oinas, J. P. Perlwitz, J. Perlwitz, D. Rind, A. Romanou, D. Shindell, P. Stone, S. Sun, N. Tausnev, D. Thresher, B. Wielicki, T. Wong, M. Yao, and S. Zhang (2005), Efficacy of climate forcings, *J. Geophys. Res.*, *110*, D18,104.

Kamae, Y., and M. Watanabe (2012), On the robustness of tropospheric adjustment in CMIP5 models, *Geophysical Research Letters*, *39*(23), doi:10.1029/2012GL054275, _eprint: https://onlinelibrary.wiley.com/doi/pdf/10.1029/2012GL054275.

Klein, S. A., and C. Jakob (1999), Validation and sensitivities of frontal clouds simulated by the ecmwf model, *Monthly Weather Review*, *127*(2), 2514âĂŞ–2531.

Klein, S. A., A. Hall, J. R. Norris, and R. Pincus (2018), Low-Cloud Feedbacks from Cloud-Controlling Factors: A Review, in *Shallow Clouds, Water Vapor, Circulation, and Climate Sensitivity*, edited by R. Pincus, D. Winker, S. Bony, and B. Stevens, pp. 135–157, Springer International Publishing, Cham, doi:10.1007/978-3-319-77273-8$_7$.

Knutti, R., D. Masson, and A. Gettelman (2013), Climate model genealogy: Generation cmip5 and how we got there, *Geophysical Research Letters*, *40*(6), 1194–1199, doi: https://doi.org/10.1002/grl.50256.

LLNL (2022), Earth system grid federation – cmip data, https://esgf-node.llnl.gov/projects/esgf-llnl/, [Dataset].

Lutsko, N. J., M. Popp, R. H. Nazarian, and A. L. Albright (2021), Emergent constraints on regional cloud feedbacks, *Geophysical Research Letters*, *48*(10), e2021GL092,934, doi: https://doi.org/10.1029/2021GL092934, e2021GL092934 2021GL092934.

Myers, T. A. (2022), Meteorological cloud radiative kernels, https://sites.google.com/site/myerstimothy/meteorological-cloud-radiative-kernels, [Computational product].

Myers, T. A., R. C. Scott, M. D. Zelinka, S. A. Klein, J. R. Norris, and P. M. Caldwell (2021), Observational constraints on low cloud feedback reduce uncertainty of climate sensitivity, *Nature Climate Change*, *11*(6), 501–507, doi:10.1038/s41558-021-01039-0.

Qin, Y., M. D. Zelinka, and S. A. Klein (2022), On the correspondence between atmosphere-only and coupled simulations for radiative feedbacks and forcing from co2, *Journal of Geophysical Research: Atmospheres*, *127*(3), e2021JD035,460, doi: https://doi.org/10.1029/2021JD035460, e2021JD035460 2021JD035460.

Ringer, M. A., T. Andrews, and M. J. Webb (2014), Global-mean radiative feedbacks and forcing in atmosphere-only and coupled atmosphere-ocean climate change experiments, *Geophysical Research Letters*, *41*(11), 4035–4042, doi: https://doi.org/10.1002/2014GL060347.

Scott, R. C., T. A. Myers, J. R. Norris, M. D. Zelinka, S. A. Klein, M. Sun, and D. R. Doelling (2020), Observed Sensitivity of Low-Cloud Radiative Effects to Meteorological Perturbations over the Global Oceans, *Journal of Climate*, *33*(18), 7717–7734, doi: 10.1175/JCLI-D-19-1028.1, publisher: American Meteorological Society Section: Journal of Climate.

Sherwood, S. C., S. Bony, O. Boucher, C. Bretherton, P. M. Forster, J. M. Gregory, and B. Stevens (2015), Adjustments in the forcing-feedback framework for understanding climate change, *Bulletin of the American Meteorological Society*, *96*(6), 217–228.

Sherwood, S. C., M. J. Webb, J. D. Annan, K. C. Armour, P. M. Forster, J. C. Hargreaves, G. Hegerl, S. A. Klein, K. D. Marvel, E. J. Rohling, M. Watanabe, T. Andrews, P. Braconnot, C. S. Bretherton, G. L. Foster, Z. Hausfather, A. S. v. d. Heydt, R. Knutti, T. Mauritsen, J. R. Norris, C. Proistosescu, M. Rugenstein, G. A. Schmidt, K. B. Tokarska, and M. D. Zelinka (2020), An assessment of Earth's climate sensitivity using multiple lines of evidence, *Reviews of Geophysics*, *n/a*(n/a), e2019RG000,678.

Smith, C. J., R. J. Kramer, G. Myhre, K. AlterskjÃęr, W. Collins, A. Sima, O. Boucher, J.-L. Dufresne, P. Nabat, M. Michou, S. Yukimoto, J. Cole, D. Paynter, H. Shiogama, F. M. O'Connor, E. Robertson, A. Wiltshire, T. Andrews, C. Hannay, R. Miller, L. Nazarenko, A. KirkevÃěg, D. OliviÃľ, S. Fiedler, R. Pincus, and P. M. Forster (2020), Effective radiative forcing and adjustments in CMIP6 models, *preprint*, Radiation/Atmospheric Modelling/Troposphere/Physics (physical properties and processes), doi:10.5194/acp-2019-1212.

Soden, B. J., A. J. Broccoli, and R. S. Hemler (2004), On the Use of Cloud Forcing to Estimate Cloud Feedback, *Journal of Climate*, *17*(19), 3661–3665, doi:10.1175/1520-0442(2004)017<3661:OTUOCF>2.0.CO;2, publisher: American Meteorological Society Section: Journal of Climate.

Soden, B. J., I. M. Held, R. Colman, K. M. Shell, J. T. Kiehl, and C. A. Shields (2008), Quantifying climate feedbacks using radiative kernels, *Journal of Climate*, *21*(6), 3504–3520.

Tan, Z., T. Schneider, J. Teixeira, and K. G. Pressel (2017), Large-eddy simulation of subtropical cloud-topped boundary layers: 2. Cloud response to climate change: LES OF LOW CLOUDS UNDER CLIMATE CHANGE, *Journal of Advances in Modeling Earth Systems*, *9*(1), 19–38, doi:10.1002/2016MS000804.

Vial, J., J.-L. Dufresne, and S. Bony (2013), On the interpretation of inter-model spread in cmip5 climate sensitivity estimates., *Climate Dynamics*, *41*(1), 3339–3362.

Webb, M., C. Senior, S. Bony, and J. J. Marcrette (2001), Combining erbe and isccp data to assess clouds in the hadley centre, ecmwf and lmd atmospheric climate models, *Climate Dynamics*, *17*(2), 905–922.

Winton, M., K. Takahashi, and I. M. Held (2010), Importance of ocean heat uptake efficacy to transient climate change, *Journal of Climate*, *23*(6), 2333–2344.

Xie, S.-P. (2020), Ocean warming pattern effect on global and regional climate change, *AGU Advances*, *1*(1), e2019AV000,130, doi:https://doi.org/10.1029/2019AV000130, e2019AV000130 2019AV000130.

Zelinka, M. (2022), Cloud radiative kernels, https://github.com/mzelinka/cloud- radiative-kernels/tree/master/data, [Computational product].

Zelinka, M. D., S. A. Klein, and K. E. Taylor (2013), Contributions of different cloud types to feedbacks and rapid adjustments in cmip5, *Journal of Climate*, *26*, 5007–5027.

Zelinka, M. D., T. A. Myers, D. T. McCoy, S. PoâĂŘChedley, P. M. Caldwell, P. Ceppi, S. A. Klein, and K. E. Taylor (2020), Causes of Higher Climate Sensitivity in CMIP6 Models, *Geophysical Research Letters*, *47*(1), e2019GL085,782.

Supporting Information for "Correlation Between Cloud Adjustments and Cloud Feedbacks Responsible for Larger Range of Climate Sensitivities in CMIP6"

N. J. Lutsko[1], M. T. Luongo[1], C. J. Wall[1], T. A. Myers[23]

Contents of this file

Corresponding author: N. J. Lutsko, Scripps Institution of Oceanography, University of California at San Diego, La Jolla, California (nlutsko@ucsd.edu)

[1]Scripps Institution of Oceanography, University of California at San Diego, La Jolla, California.

[2]Cooperative Institute for Research in Environmental Sciences (CIRES), University of Colorado, Boulder, Colorado, USA

[3]Physical Science Laboratory, National Oceanic and Atmospheric Administration, Boulder, Colorado, USA

1. Text S1

2. Figures S1 and S2

Introduction The supplementary material contains a description of the Cloud Controlling Factor analysis in test S1 and two figures. Figure S1 compares different methods of estimating radiative forcing in CMIP5 and CMIP6. Figure S2 breaks down the different components of the Cloud Controlling Factor analysis.

Text S1. Cloud Controling Factor Analysis To investigate how changes in governing meteorological conditions contribute to low cloud adjustments, we perform a cloud controlling factor (CCF) analysis [e.g., *Klein et al.*, 2018; *Scott et al.*, 2020]. The basic assumption of a CCF analysis is that the change in some property of low clouds, for example the low cloud radiative effect, R, in response to a forcing (Δ, taken here to be abrupt 4xCO2 forcing), can be represented as a first-order Taylor expansion in CCFs, x_i:

$$\Delta R = \sum_i \frac{\partial R}{\partial x_i} \Delta x_i. \tag{1}$$

Above, the partial derivatives are the sensitivity of R to respective CCFs (i.e. meteorological cloud radiative kernels) and are assumed to be time-scale invariant. The Δx_i terms are the change in the CCF fields due to the forcing. According to *Klein et al.* [2018], the six meteorological CCF fields with the biggest impact on low clouds are sea surface temperature (SST), estimated inversion strength (EIS), horizontal temperature advection (Tadv), 700 hPa pressure velocity (ω700), 700 hPa relative humidity (RH700), and wind speed (WS), with SST and EIS having considerably more influence than the others. Hence the change in low cloud radiative effect can be decomposed into a sum of six terms:

$$\Delta R = \frac{\partial R}{\partial SST}\Delta SST + \frac{\partial R}{\partial EIS}\Delta EIS + \frac{\partial R}{\partial Tadv}\Delta Tadv + \frac{\partial R}{\partial \omega 700}\Delta \omega 700 + \frac{\partial R}{\partial RH700}\Delta RH700 + \frac{\partial R}{\partial WS}\Delta WS. \tag{2}$$

In this study, we focus on low cloud adjustments, so ΔSST=0 and all other variables are taken from FixedSST experiments.

Meteorological Cloud Radiative Kernels

We use meteorological cloud radiative kernels ($\partial R/\partial x_i$) from *Myers et al.* [2021], as well as a new kernel for CESM2 that was not included in their analysis. These kernels were calculated from 20 (for CMIP5) or 50 years (for CMIP6) of a preindustrial control GCM simulation according to the method presented in *Scott et al.* [2020] and provide the GCM-simulated low cloud-induced change in TOA radiative flux per unit change in cloud-controlling factor x_i. Note that due to data limitations, the CESM2 meteorological cloud radiative kernel was calculated from 50 years of a historical simulation. These data are presented on a $5° \times 5°$ grid from 60°S-60°N and have units of W m $^{-2}$ dx_i^{-1}.

Meteorological Predictor Fields

We use monthly mean output from a control and an abrupt4xCO2 FixedSST experiment for CMIP5 (sstClim & sstClim4xCO2, respectively) and CMIP6 (piClim-control & piClim-4xCO2, respectively). We calculate Δx_i by taking the thirty-year average difference between the abrupt forcing run and the control run.

ω700, RH700, and WS are standard GCM outputs. Following *Scott et al.* [2020], EIS can be calculated from monthly mean GCM outputs as:

$$EIS = LTS - \Gamma_m^{850}(Z_{700} - Z_{LCL}), \tag{3}$$

where LTS is lower-tropospheric stability (the difference in potential temperature between 700 hPa and the surface), Γ_m^{850} is the moist-adiabatic lapse rate at 850 hPa, Z_{700} is the height of the 700 hPa pressure level relative to the surface, and Z_{LCL} is the height of the lifting condensation level relative to the surface.

Similarly, we follow *Scott et al.* [2020] to calculate Tadv as:

$$Tadv = -\frac{U_{10}}{a\cos(\phi)}\frac{\partial SST}{\partial \lambda} - \frac{V_{10}}{a}\frac{\partial SST}{\partial \phi}, \tag{4}$$

which uses a second-order centered finite-difference scheme where U_{10} and V_{10} are the zonal and meridional 10m wind components, ϕ is latitude, λ is longitude, and a is Earth's mean radius.

Note that the NCAR model does not output 10m wind components. As a work-around, we follow *Vimont et al.* [2009] and *Hwang and Chung* [2021] who estimate the 10m wind vectors by taking the average of the 1000 hPa and 850 hPa level winds and multiply it by 80%. In addition, near-surface wind speed is not output by CCSM4. Unfortunately the monthly average surface wind speed, found by taking the average of surface wind speeds at each time step over the course of the month, is not the same as taking the magnitude of the monthly average surface wind vector. Because WS is not a major driver of cloud adjustment [e.g. *Klein et al.* [2018] and results from other models below], we set the ΔWS term to NaN in our CCSM4 calculations and proceed.

Error Estimation

We calculate 95% uncertainty based on *Myers et al.* [2021]. At each grid box, we give the 95% confidence interval as,

$$\frac{\partial R}{\partial x_i}\Delta x_i \pm t\sqrt{\Delta \mathbf{x}_i^T C \Delta \mathbf{x}_i}\sqrt{\frac{N_{nom}}{N_{eff}}} = \frac{\partial R}{\partial x_i}\Delta x_i \pm \delta. \tag{5}$$

Above, C is the covariance matrix of regression coefficients at each grid cell from *Myers et al.* [2021]'s meteorological radiative kernels, $\Delta \mathbf{x}_i$ is a 7×1 vector of the six Δx_i values and a one (note that we set the SST value to 0), and N_{nom}/N_{eff} is the ratio of the nominal to effective number of monthly values. For N_{nom}, we note that *Myers et al.* [2021] used data from July 1983-December 2018 and for N_{eff} we divide N_{nom} by 5 following *Myers et al.* [2021]'s rule of thumb that "we find that one out of five points is independent temporally." t is the critical value of the Student's t-test at the 95% significance level with $N_{eff} - 6$ degrees of freedom. Note that in *Myers et al.* [2021], they consider the critical t value for $N_{eff} - 7$ degrees of freedom, but because we remove SST from our analysis we consider only six.

This gives us an uncertainty at each grid cell. We calculate the global mean (denoted by angular brackets) error for each model (s) as,

$$\langle \frac{\partial R}{\partial x_i} \Delta x_i \rangle \pm \sqrt{\frac{\sum_k (\delta_k w_k)^2}{(\sum_k w_k)^2}} \sqrt{\frac{N^*_{nom}}{N^*_{eff}}} = \langle \frac{\partial R}{\partial x_i} \Delta x_i \rangle \pm s, \tag{6}$$

where δ_k is the uncertainty in the k-th grid box, w_k is the cosine of ϕ, and N^*_{nom}/N^*_{eff} is the ratio of nominal to effective number of $5° \times 5°$ grid boxes, taken here to be 30 per *Myers et al.* [2021]'s rule of thumb: "around 1 out of 30 grid boxes is independent."

Lastly, we take the global mean error for each model and calculate the multi-model mean error as,

$$s_{MMM} = \left(\sqrt{s_1^2 + \ldots + s_n^2} \right) / n, \tag{7}$$

where n is the number of models (in our case, six for CMIP5 and seven for CMIP6).

References

Hwang, Y.-T., and P.-C. Chung (2021), Seasonal Sensitivity of the Cross-Equatorial Hadley Cell Response to Extratropical Thermal Forcings, *Journal of Climate*, *34*, 3327–3342, doi:10.1175/JCLI-D-19-0938.1, publisher: American Meteorological Society Section: Journal of Climate.

Klein, S. A., A. Hall, J. R. Norris, and R. Pincus (2018), Low-Cloud Feedbacks from Cloud-Controlling Factors: A Review, in *Shallow Clouds, Water Vapor, Circulation, and Climate Sensitivity*, edited by R. Pincus, D. Winker, S. Bony, and B. Stevens, pp. 135–157, Springer International Publishing, Cham, doi:10.1007/978-3-319-77273-87.

Myers, T. A., R. C. Scott, M. D. Zelinka, S. A. Klein, J. R. Norris, and P. M. Pincus (2021), Observationa Constraints on Low-Cloud Feedback Reduce Uncertainty of Climate Sensitivity, *Nature Climate Change*, *11*, 501–507, doi:10.1038/s41558-021-01039-0.

Scott, R. C., T. A. Myers, J. R. Norris, M. D. Zelinka, S. A. Klein, M. Sun, and D. R. Doelling (2020), Observed Sensitivity of Low-Cloud Radiative Effects to Meteorological Perturbations over the Global Oceans, *Journal of Climate*, *33*(18), 7717–7734, doi:10.1175/JCLI-D-19-1028.1, publisher: American Meteorological Society Section: Journal of Climate.

Vimont, D. J., M. Alexander, and A. Fontaine (2009), Midlatitude Excitation of Tropical Variability in the Pacific: the Role of Thermodynamic Coupling and Seasonality, *Journal of Climate*, *22*, 518–534, doi:10.1175/2008JCLI2220.1, publisher: American Meteorological Society Section: Journal of Climate.

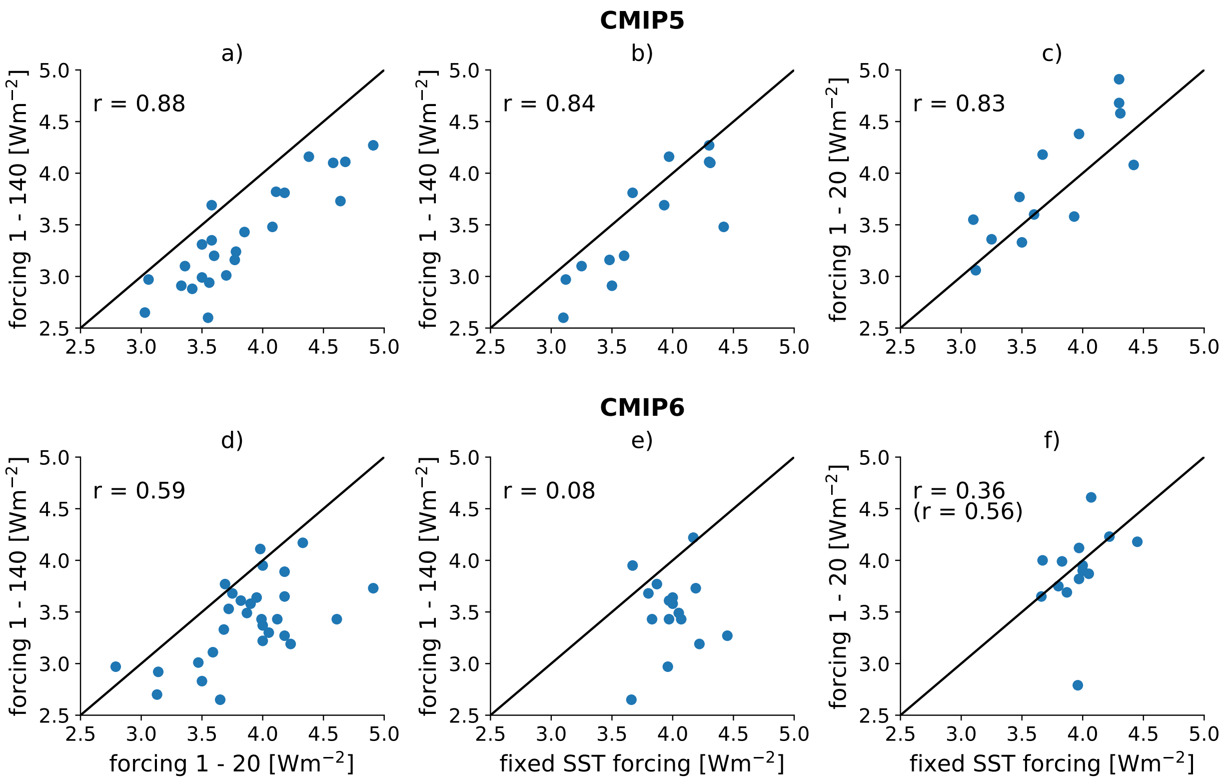

Figure S1. Comparisons of different methods of estimating radiative forcing in CMIP5 and CMIP6. a) F_{1-140} versus F_{1-20} in CMIP5, b) F_{1-140} versus F_{fix} in CMIP5, c) F_{1-20} versus F_{fix} in CMIP5, d) F_{1-140} versus F_{1-20} in CMIP6, e) F_{1-140} versus F_{fix} in CMIP6, f) F_{1-20} versus F_{fix} in CMIP6. In all panels the Pearson correlation coefficient r is shown in the upper left and the black lines show the 1:1 line. The text in brackets in panel f) gives the Pearson correlation coefficient when CNRM-ESM2.1 (the outlier with anomalously small F_{1-20}) is excluded from the correlation.

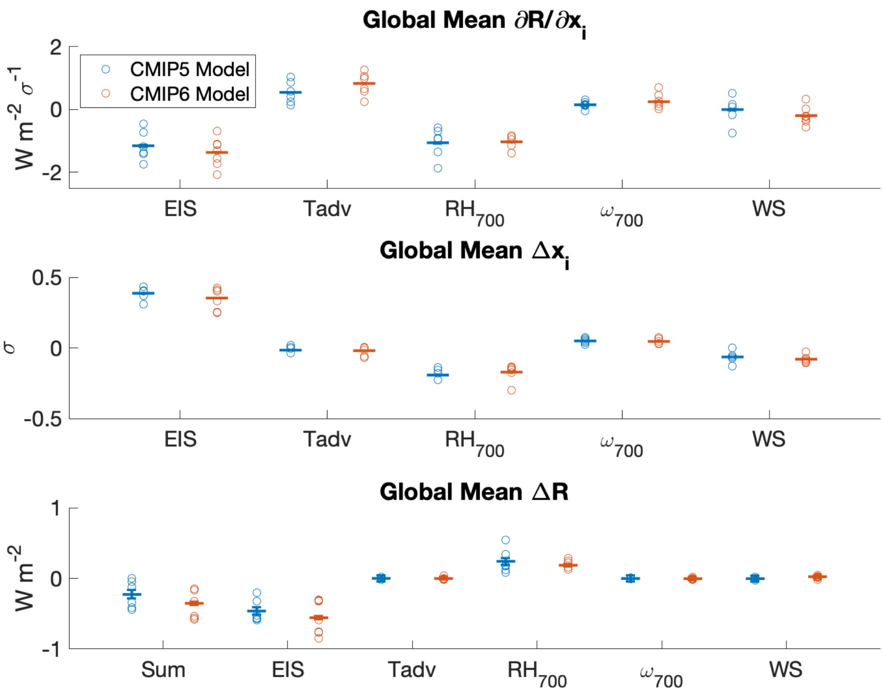

Figure S2. Results of the CCF analysis. The top panel show the global-mean values of the meteorological cloud radiative kernels for the CMIP5 and CMIP6 models (blue and red circles, respectively), which demonstrates how the sensitivity of the CRE R to the meteorological controling factors varies between the model generations. The middle panel shows the global-mean responses of the meteorological controling factors to quadrupling of CO_2, in units of per standard deviation. The bottom panel shows the total change in CRE ΔR estimated from the CCF analysis ("Sum"), as well as the contributions from the individual CCF fields. The error bars show the multimodel mean error.